Evaluation of Fast Diffusion Kurtosis Imaging Using New Software Designed for Widespread Clinical Use

by Irfan Sugianto

Submission date: 20-Sep-2022 04:00PM (UTC+0700)
Submission ID: 1904393320
File name: uation_of_Fast_Diffusion_Kurtosis_Imaging_Using_New_Software.pdf (2.56M)
Word count: 6344
Character count: 31482

Acta Med. Okayama, 2022
Vol. 76, No. 3, pp. 297-305

Acta Medica Okayama
http://escholarship.lib.okayama-u.ac.jp/amo/

Original Article

Evaluation of Fast Diffusion Kurtosis Imaging Using New Software Designed for Widespread Clinical Use

Masahiro Kuroda[a*§], Kohei Konishi[a§], Kohei Sugimoto[a], Yuuki Yoshimura[a,b], Kentaro Hamada[a], Abdullah Khasawneh[c], Majd Barham[c], Nouha Tekiki[c], Irfan Sugianto[c,d], Babatunde O. Bamgbose[c,e], Hinata Ishizaki[c], Yudai Shimizu[c], Yuki Nakamitsu[a], Wlla E. Al-Hammad[c], Ryo Kamizaki[a], Akira Kurozumi[f], Toshi Matsushita[f], Seiichiro Ohno[f], Susumu Kanazawa[g], and Junichi Asaumi[c]

[a]*Radiological Technology, Graduate School of Health Sciences, Okayama University,*
Departments of [c]Oral and Maxillofacial Radiology, [g]Radiology, Okayama University Graduate School of Medicine, Dentistry and Pharmaceutical Sciences, [f]Central Division of Radiology, Okayama University Hospital, Okayama 700-8558, Japan,
[b]Radiology Diagnosis, Okayama Saiseikai General Hospital, Okayama 700-8511, Japan,
[d]Department of Oral Radiology, Faculty of Dentistry, Hasanuddin University, Makassar, Indonesia,
[e]Department of Oral Diagnostic Sciences, Faculty of Dentistry, Bayero University, Kano, Nigeria

Clinical research using restricted diffusion-weighted imaging, especially diffusion kurtosis (DK) imaging, has been progressing, with reports on its effectiveness in the diagnostic imaging of cerebral infarctions, neurodegenerative diseases, and tumors, among others. However, the application of DK imaging in daily clinical practice has not spread because of the long imaging time required and the use of specific software for image creation. Herein, with the aim of promoting clinical research using DK imaging at any medical facility, we evaluated fast DK imaging using a new software program. We developed a new macro program that produces DK images using general-purpose, inexpensive software (Microsoft Excel and ImageJ), and we evaluated fast DK imaging using bio-phantoms and a healthy volunteer in clinical trials. The DK images created by the new software with diffusion-weighted images captured with short-time imaging sequences were similar to the original DK images captured with long-time imaging sequences. The DK images using three *b*-values, which can reduce the imaging time by 43%, were equivalent to the DK images using five *b*-values. The DK imaging technique developed herein might allow any medical facility to increase its daily clinical use of DK imaging and easily conduct clinical research.

Key words: fast diffusion kurtosis imaging, mean kurtosis, restricted diffusion, Excel, ImageJ

Diffusion-weighted (DW) images represent the degree of Brownian motion of water molecules in a living body. In an apparent diffusion coefficient (ADC) map, which is created by DW images, the ADC value is calculated as the slope of a straight line obtained from the signal intensities in DW images taken with two or more different b-values. ADC maps are indispensable for the diagnosis of cerebral infarctions and tumors in daily practice [1-4]. In recent years, restricted diffusion-weighted imaging — especially diffusion kurtosis (DK) imaging — has been attracting attention, and clinical research using these imaging modalities is in

Received March 18, 2021; accepted January 18, 2022.
*Corresponding author. Phone: +81-86-235-6873; Fax: +81-86-235-6873
E-mail: kurodamd@cc.okayama-u.ac.jp (M. Kuroda)
§These authors contributed equally to this work.

Conflict of Interest Disclosures: No potential conflict of interest relevant to this article was reported.

progress. There have been reports of the effectiveness of DK imaging in the diagnostic imaging of cerebral infarctions, neurodegenerative diseases, and tumors, among others [5-9]. However, the imaging time that is needed to obtain DW images for DK imaging is significantly longer than that needed for ADC maps, because DW images for DK imaging are usually taken for all 30-axis directions with three or more different b-values [5, 10-12]. In addition, specific and expensive software, such as MATLAB, is required for image creation. For these reasons, the clinical application of DK imaging has not yet progressed.

We conducted the present study to evaluate fast DK imaging that uses a new DK imaging software program that is intended for widespread use in clinical practice. This software uses macro functions of general-purpose inexpensive software such as Microsoft Excel and ImageJ, and it produces a DK image using three-axis DW images that are taken over a short time period to create ADC maps in daily clinical practice. This approach could enable any medical facility to obtain ADC maps as well as DK images simultaneously using the same DW images. We tested the new fast DK imaging and DK imaging software with both bio-phantoms and a healthy human volunteer.

Materials and Methods

Phantoms. Jurkat cells purchased from Bio Resource Center (Tsukuba, Japan) were used to create bio-phantoms. Cultures were carried out in RPMI 1640 medium (pH 7.4; Gibco/Thermo Fisher Scientific, Waltham, MA, USA) with 10% fetal bovine serum (Filtron, Victoria, Australia) and 1% penicillin-streptomycin-neomycin (Gibco/Thermo Fisher Scientific). Incubation was performed at 37°C with 5% CO_2. After the number of Jurkat cells was measured, the cell solution was concentrated and adjusted to approx. 8×10^8 cells/ml in a micro-cuvette (Halbmikro 1.5 ml; Greiner Labortechnik Manufacturing, Düsseldorf, Germany). The cells were encapsulated within gellan gum (P-8169; Sigma-Aldrich, St. Louis, MO) to prepare bio-phantoms of 7.4×10^8 cells/ml. As a control, a phantom containing 0.9% physiological saline was prepared.

The phantoms were placed in a phantom container measuring 9.5 cm in length, 14 cm in width and 7 cm in height. The interior of the container was filled with physiological saline [13, 14]. These bio-phantoms using Jurkat cells had an ADC value of ~0.6×10^{-3} mm^2/sec and a mean kurtosis value of ~1.3, mimicking the values of human tumor tissues [14, 15].

Healthy volunteer and ethical approval. Human images were obtained from a healthy volunteer. This study was approved by the Ethics Committee of the Okayama University Graduate School of Medicine, Dentistry and Pharmaceutical Sciences, Okayama University Hospital (approval no. RIN1910-004), and written consent was obtained from the volunteer.

Magnetic resonance (MR) imaging.

1. MRI system. A 3T MRI system (Magnetom Prisma VE11C; Siemens, Munich, Germany) and a 1.5T MRI system (Magnetom Avanto fit VE11C; Siemens) with a 20-channel head/neck coil were used. The 3T MRI system was used to image the phantoms, and the 1.5T MRI system was used to image the human body.

2. Temperature control during MR imaging. The phantom container was installed in an in-house heating device made of ethylene-vinyl acetate copolymer. The heating device was connected to a circulating constant temperature bath (Thermo-Mate BF-41; Yamato Scientific Co., Tokyo). To replicate human body temperature, the inside of the phantom container was heated to approx. 37°C. During the MRI scanning, the phantom temperature was adjusted using an optical fiber thermometer (Fluoroptic™ m3300, Luxtron Co., Santa Clara, CA, USA) to maintain a constant temperature of 37°C.

3. Phantom imaging. DW images of the phantoms were acquired using multiple imaging sequences, as shown in Table 1. Concerning on imaging conditions, in a DW image taken using a b-value >1000, water signal value drops to noise level, and the MK value of water, which should theoretically be 0, is calculated to be higher than 0 (data not shown). We therefore set the maximum b-value as 1000. For the DK imaging, single shot-echo planar imaging (SS-EPI) was used in three sequences, *i.e.*, DKI-1, DKI-2, and DKI-3 (Table 1) based on the recommended DKI protocols for Siemens scanners; Tim Trio (long) <https://medicine.musc.edu/-/sm/medicine/departments/f/tim-trio-long.ashx?la=en> (accessed Oct. 15, 2020), with the parametric tensor 'off' selected. The number of diffusion directions was 30. Readout segmentation of long variable echo-train (RESOLVE) sequences were used for fast diffusion kurtosis imaging using new software.

Table 1 Diffusion-weighted (DW) imaging conditions for the Diffusional Kurtosis Estimator (DKE) images and several diffusion kurtosis (DK) images of the bio-phantoms

Target images	DKE image, DKI-H		DKI-M
Sequences	DKI-1 & DKI-2	DKI-3	RESOLVE
Parameters			
TR (msec)	6000	6000	8000
TE (msec)	75	75	86
ES (msec)	0.93	0.93	0.56
FOV (mm)	120	120	120
Matrix	82 × 82	82 × 82	224 × 224
BW (Hz/pixel)	1220	1220	399
Averages	1	9	2
Segments	1	1	7
Slice thickness (mm)	5	5	5
Slice number	5	5	1
b-value (sec/mm^2)	0, 500, 1,000	0	0, 500, 1,000
Diffusion direction	30	–	3
Imaging time (min : sec)	6 : 24	1 : 12	13 : 28

DKE image, DKI created by DKE software using DW images with DKI-1, DKI-2 and DKI-3; DKI-H, DKI created by in-house DK imaging software using DW images with DKI-1, DKI-2 and DKI-3 sequences; DKI-M, DKI created by in-house DK imaging software using DW images with RESOLVE sequence. DKE, Diffusional Kurtosis Estimator; DKI, diffusion kurtosis image; RESOLVE, readout segmentation of long variable echo-trains; TR, repetition time; TE, echo time; ES, echo space; FOV, field of view; BW, band width; DW, diffusion-weighted; DK, diffusion kurtosis.

4. Human body imaging. A DW image of the volunteer's brain was obtained. Two types of imaging sequences (Table 2) were used to examine the possibility of shortening the imaging time in clinical practice. RESOLVE-5 and RESOLVE-3 were created as protocols with long and short imaging times respectively, depending on the number of *b*-values. Due to the Ethics Committee's recommendation, long-time imaging (DKE imaging) was not performed on the volunteer. Concerning on imaging conditions, in a DW image taken using a *b*-value >1000, water signal value drops to noise level, and the MK value of water, which should theoretically be 0, is calculated to be higher than 0 (data not shown). Therefore, the maximum *b*-value was set as 1000.

Development of the DK imaging software. The software used to create a DK image was developed in-house as a combination of macro programs of the inexpensive general-purpose software Microsoft Excel (2016, Microsoft, Redmond, WA) and ImageJ (ver. 1.52a; U.S. National Institutes of Health, Bethesda, MD). The new software calculates the mean kurtosis (MK) values for each pixel according to the principle of DK imaging using the signal value of each pixel of the DW images with several *b*-values, and it then creates a DK image.

Table 2 Diffusion-weighted (DW) imaging conditions for the diffusion kurtosis (DK) images of the human brain

Sequences	RESOLVE-3	RESOLVE-5
Parameters		
Imaging time (min : sec)	1:57	3:24
b-value (sec/mm^2)	0, 500, 1,000	0, 250, 500, 750, 1,000
TR (msec)	4860	4860
TE (msec)	76	76
ES (msec)	0.44	0.44
FOV (mm)	220	220
Matrix	140 × 140	140 × 140
BW (Hz/pixel)	1116	1116
Averages	1	1
Segments	3	3
Slice thickness (mm)	5	5
Slice number	23	23
Diffusion direction	3	3

RESOLVE, readout segmentation of long variable echo-trains; TR, repetition time; TE, echo time; ES, echo space; FOV, field of view; BW, band width.

Equation (1) explains the relationship between the signal value, MK value, and ADC value of each pixel of the DW image captured with each *b*-value, which is necessary for calculating the MK value [7]. Here, MK

is one of the parameters of DK.

$$S(b) = S_0 \exp\left(-bADC + \frac{1}{6}b^2ADC^2\,MK\right) \quad (1)$$

Here, S is the signal value at a certain pixel position, b is the b-value used, and S_0 is the signal value when a motion probing gradient at the same pixel position is not applied; *i.e.*, when the b-value is 0. ADC is the ADC value at the pixel position, and MK is the MK value at the pixel position.

Specifically, according to the schematic diagram in Fig. 1, the DW images with different b-values were opened as DICOM images and then saved as text files using ImageJ as Step 1. Next, in Step 2, each text file was read using both Microsoft Excel and an Excel sheet in which the logarithm of the signal value at each pixel of each image was saved. For the pixels at the same position in each image, the b-value was plotted as 'x' on the horizontal axis, and the logarithmic signal value was plotted as 'y' on the vertical axis. Using the Linest function on the quadratic function $y = Ax^2 + Bx + C$, the coefficients A and B were calculated for each pixel and saved in the Excel sheet. From the coefficients A and B, the MK value was calculated for each pixel using Equation (2) and saved as a text file. The MK value was replaced with 0 if the calculated MK value became negative.

$$MK = 6A/(-B)^2 \quad (2)$$

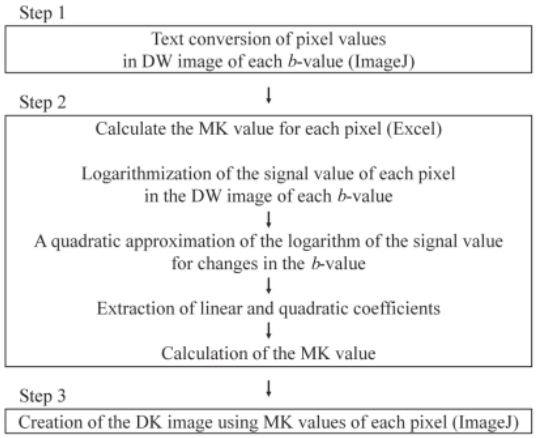

Fig. 1 Flowchart of the calculation steps of the diffusion kurtosis (DK) imaging software based on the mean kurtosis (MK) used in this study. DW: diffusion-weighted.

Finally, in Step 3, the text file with MK values was converted into tiff format and saved as a DK image using ImageJ. In this DK imaging software, the macro functions of ImageJ were used for Steps 1 and 3, and the macro functions of Excel VBA were used for Step 2. Using this software, DW images were imported, the MK values were calculated, and finally, a DK image was created automatically.

Evaluation of the DK imaging software. To evaluate the accuracy of the calculation of the DK imaging software, we prepared three DW images with the b-values 0, 500, and 1000 as shown in Fig. 2. For the DW images obtained with the b-values 0 and 1000, the signal values of all pixels in each DW image were set to 2000 and 1300, respectively. For the DW image obtained with the b-value 500, four signal values of pixels were set: 1612, 1598, 1576, and 1535. Using the DK imaging software, the MK value of each pixel was calculated and compared with the theoretical value.

Diffusional Kurtosis Estimator (DKE) for comparison with the DK imaging software. We used the DKE software ver. 2.6 <https://medicine.musc.edu/departments/centers/cbi/dki> (accessed Oct. 15, 2020)

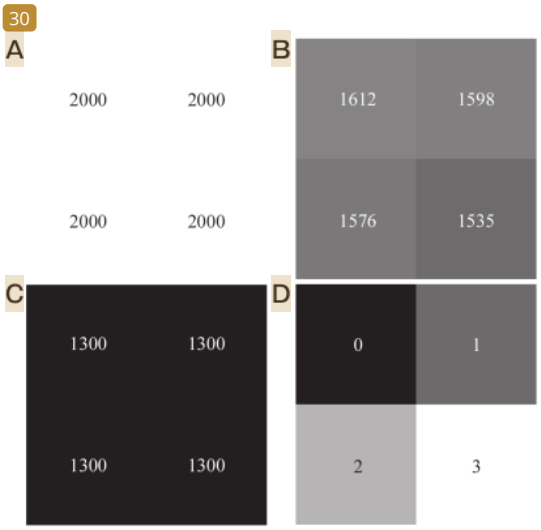

Fig. 2 Evaluation of the DK imaging software. (**A**) DW image with 0 s/mm² b-value. The signal values of all pixels were set to 2000. (**B**) DW image with the b-value 500. The signal values of pixels were set to 1612, 1598, 1576, and 1535. (**C**) DW image with the b-value 1000. The signal values of all pixels were set to 1300. (**D**) DK image created using the DK imaging software. All MK values in each pixel with the range between 0 and 3 were identical to the theoretical values.

for a comparison with the DK imaging software. To create DK images, the MK value for each pixel was calculated using DWIs of DKI-1, DKI-2, and DKI-3, according to the theoretical description of 'DKI protocols' <https://medicine.musc.edu/departments/centers/cbi/dki/protocols> (accessed Oct. 15, 2020).

DK image of phantoms. Three types of DK images (Table 1) were created for the phantoms. A DK image created by DKE software using a 30-axis DW image captured by DKI-1, DKI-2, and DKI-3, which are dedicated sequences for DKE software, was defined as the DKE image. The DK image created by the in-house DK imaging software using the 30-axis DW images calculated from DKI-1, DKI-2, and DKI-3 by DKE was defined as DKI-H. The DK image created by the in-house DK imaging software using the three-axis DW images captured by the RESOLVE sequence [16,17] to reduce image distortion was defined as DKI-M. The resolutions of the DKE image, DKI-H, and DKI-M were 120×120, 82×82, and 224×224, respectively.

DK image of the human body. Two DK images (Table 2) were created for the human body. The DK image of the volunteer's brain was created and defined as DKI-M, using the in-house DK imaging software and the three-axis DW images captured by RESOLVE-5, which is a long-time protocol, and RESOLVE-3, which is a short-time protocol.

Image analysis and statistics. For the quantitative test of the similarity of the multiple DK images of the phantoms, we changed the resolutions of the DKE image and DKI-H and unified them from 120×120 and 82×82 into 224×224, respectively, so as not to change the signal value of each pixel using the "resize without interpolation" function of ImageJ. We then evaluated the pixel values at the same pixel position in the region of interest (ROI) of each image by determining the Spearman's rank correlation coefficient (BellCurve for Excel; Social Survey Research Information Co., Tokyo). Spearman's rank correlation coefficients were calculated between DKE and each DKI for the merged ROI of each bio-phantom and the physiological saline part of each 5×17 pixel. In the significance test of rank correlation coefficients, a p-value <0.05 was accepted as significant. For the quantitative test in the human study, Spearman's rank correlation coefficients were calculated for the ROIs of the whole brain part to evaluate the similarity of DKI-Ms using RESOLVE-3 and RESOLVE-5. In the significance test of the rank correlation coefficient, a p-value <0.05 was accepted as significant.

Results

The accuracy of calculation of the DK imaging software. Figure 2A-C shows DW images obtained with the b-values 0, 500 and 1000, and Fig. 2D provides a DK image created by the DK imaging software. All MK values of pixels in the DK image were identical to the theoretical values calculated using Equations 1 and 2.

The evaluation of DK images of the phantoms. DK images of the phantoms are given in Fig. 3; the figure panels A and B are a DKE image and DKI-H created with DKE software and the in-house DK imaging software from 30-axis DW images captured using DKI-1, DKI-2, and DKI-3, respectively. Figure 3C is a DKI-M created using the in-house DK imaging software and three-axis DW images captured by RESOLVE. We used the DKE image as the gold standard DK image and compared it with the other DK images.

Regarding the MK values of the bio-phantom and the physiological saline part, the DK images were visually similar to the DKE image. The DKI-M was better than the DKE image and DKI-H concerning the depiction of the phantom structure, although salt-and-pepper noise was observed in the DKI-M. The MK values (mean ± SD) of the physiological saline part and bio-phantom part were 0.0 ± 0.0 and 1.2 ± 0.1 in the DKE image and 0.1 ± 0.1 and 0.9 ± 0.5 in the DKI-M, respectively.

Table 3 lists the data of the quantitative evaluation of

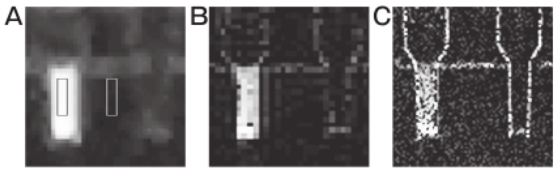

Fig. 3 Diffusion kurtosis (DK) images of the phantoms. Bio-phantom (*left*) and physiological saline (*right*) were used as phantoms. (**A**) Diffusional Kurtosis Estimator (DKE) image created with the DKE software and diffusion-weighted (DW) images taken using DKI-1, DKI-2, and DKI-3 sequences. *Black squares* and *white squares* indicate the positions of ROIs for the bio-phantom and physiological saline, respectively. (**B**) DKI-H created with the in-house DK imaging software and DW images taken using DKI-1, DKI-2, and DKI-3 sequences. (**C**) DKI-M created with the in-house DK imaging software and DW images taken using a RESOLVE (readout segmentation of long variable echo-train) sequence.

Table 3 Spearman's rank correlation coefficient of each diffusion kurtosis (DK) image for the Diffusional Kurtosis Estimator (DKE) image: Bio-phantom study

Images	DKI-H	DKI-M
Spearman's rank correlation coefficients	0.84	0.67
Significance testing for each Spearman's rank correlation coefficient	$P<0.001$	$P<0.001$

DKI-H, DKI created by in-house DK imaging software using DW images with DKI-1 & DKI-2 and DKI-3 sequences; DKI-M, DKI created by in-house DK imaging software using DW images with RESOLVE sequence. Spearman's rank correlation coefficients were calculated between DKE and each DKI for the merged region of interest of bio-phantom and physiological saline part of each 5 × 17 pixels. Each p value shows the test result for the correlation coefficient between DKE and each DKI.
DKI, diffusion kurtosis imaging; DK, diffusion kurtosis; DW, diffusion-weighted; RESOLVE, readout segmentation of long variable echo-trains; DKE, diffusional kurtosis estimator.

the similarity of the MK values in various DK images shown in Fig. 3. The Spearman's rank correlation coefficients for the correlation between the MK value at each pixel position of the DKE image and the MK value at the same pixel position of other DK images (DKI-H, DKI-M) were within the range of 0.67 and 0.84, with significant correlations ($p<0.001$), indicating quantitatively high similarity.

The evaluation of DK images of the human body. DK images of the volunteer's brain are shown in Fig. 4. The figure's panels A and B are DKI-Ms created by the in-house DK imaging software and the DW images captured with the RESOLVE-3 and RESOLVE-5 sequences in Table 2, respectively. In the DKI-M, the MK values and the depiction of brain structure were similar between panels A and B of Fig. 4, although roughness due to salt-and-pepper noise was observed to the same extent in both. The scatter plot (Fig. 4C) illustrating the relationship between the MK values at the same pixel position of Fig. 4A and 4B indicates the similarity of DKI-Ms using RESOLVE-3 and RESOLVE-5. The Spearman's rank correlation coefficient for Fig. 4C was 0.88 with a significant correlation ($p<0.001$), indicating quantitatively high similarity.

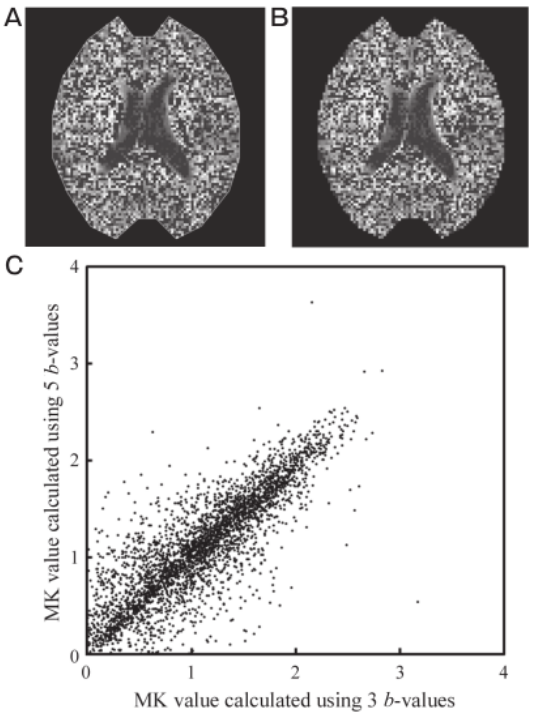

Fig. 4 DKI-Ms of the human brain. (**A**) DKI-M created with the in-house DK imaging software and DW images taken using a RESOLVE-3 sequence. *White line* around brain indicates the position of the ROI for the whole brain. (**B**) DKI-M created with the in-house DK imaging software and DW images taken using a RESOLVE-5 sequence. (**C**) The scatter plot of the relationship between the MK values at the same pixel position of panels (A) and (B) in the ROI for the whole brain.

Discussion

We evaluated fast DK imaging using a new software program that produces DK images using macro functions of the inexpensive general-purpose software Excel and ImageJ. The new software uses DW images captured for creating the ADC map in daily clinical practice, and it enables the creation of both the ADC map and the DK image at the same time, in a relatively short period of time. This can be performed in any medical facility. The DK image created by the new software using DW images that were captured with three *b*-values and three axes was similar to the original DK image that was created over a relatively longer imaging time with 30 axes. With the new software, DK imaging and clinical research can thus be performed in daily clinical practice at any medical facility.

Clinical research on restricted diffusion-weighted imaging, especially DK imaging, has progressed in

recent years. DK imaging is available for the diagnosis of ischemic stroke such as cerebral thrombosis and cardiogenic cerebral infarction [5], neurodegenerative diseases such as Parkinson's disease and Alzheimer's dementia [6,7], and tumors such as prostate cancer and osteosarcoma [8,9]. It has become common to create DK images with processing by MATLAB-based software using DW images captured with 15 or 30 axes and three or more different *b*-values [5,10-12]. The imaging time of DW images in these clinical studies has been as long as 6-8 min [5,12,18,19]. In contrast, the imaging time needed to obtain DW images for the ADC maps that are taken in daily clinical practice with three *b*-values and three axes is usually as short as 1-2 min [20]. Our present study evaluated DK images for which the imaging time was as short as 2 min. In most clinical studies of DK imaging, the imaging time of DW images is significantly longer than that of ADC maps [5,12,18,19]. In addition, the software for creating DK images is not widespread since few products are commercialized, and most clinical trials use in-house software [5,10-12]. For these reasons, the clinical research and clinical spread of DK imaging are still limited.

Many methods to reduce the number of imaging axes and the number of *b*-values of DW imaging have been tested with the goal of shortening the DK imaging time [21,22]. The DW imaging time is 6-8 min for the original 30 axes and three *b*-values [5,12,18,19], approx. 3 min for 15 axes and three *b*-values [21], approx. 4 min for three axes and six *b*-values [9], and approx. 5 min for three axes and four *b*-values [22]. In the present study, the imaging time was shortened to approx. 2 min with three axes and three *b*-values. Regarding the number of *b*-values for three-axis imaging, Pasicz *et al.* [22] compared seven *b*-values and four *b*-values for short-time imaging of the liver and pancreas of healthy volunteers, and they reported that the parameters of DK images with four *b*-values were the same as those with seven *b*-values, indicating the possibility of short-time DK imaging. In our present investigation as well, the MK values of the DK image with three *b*-values, which can reduce the imaging time by 43% compared to the use of five *b*-values, is similar to those with five *b*-values, also indicating the possibility of short-time DK imaging.

As DKE calculates DK images using DW images with 30 axes, DK imaging with 30 axes took a long time. The resolution of a DK image of the phantom was thus limited to 120×120 to shorten the imaging time. DK imaging by our new software using DW images captured with three axes and a RESOLVE sequence [16] has the advantage of fast and high-resolution imaging, resulting in better depictions of phantom structures than the depictions provided by DKE images.

We selected 1000 for the maximum *b*-value in order to acquire DKI at the same time as the ADC map, as it is recommended that the ADC map in daily clinical practices should be created using DW images taken with *b*-values of 1000 or less [23]. For DK imaging, the maximum *b*-value of 1000 is rather low [23], but several recent clinical papers using the maximum *b*-value of 1000 have confirmed the usefulness of DKI for prostate cancer [24,25] and renal tumors [26-28]. Wu *et al.* [29] and Zhang *et al.* [30] indicated that DKI with the low maximum *b*-value of 1400 is useful for the diagnosis of prostate cancer. Regarding the number of diffusion imaging directions of DKI, there are many papers reporting the clinical usefulness of three-axis imaging of DKI, and the review by Rosenkrantz *et al.* [23] stated that the three-axis direction is sufficient as the number of imaging directions.

We developed the in-house DK imaging software as software written in a macro language that runs Excel and ImageJ, which are inexpensive and available to everyone; they can be obtained at a much lower price than MATLAB, which is often used in clinical research of DK imaging, and they are easy to manage for version upgrades; they can thus be used at any medical facility to create DK images. The new software may contribute to future clinical research on DK imaging. To the best of our knowledge, this is the first paper using the free software ImageJ to produce DK images.

One limitation of this software is that it saves DK images in the tiff format instead of DICOM, although medical images are usually saved in an image server in the DICOM format. For conversion to the DICOM format, it is necessary to add a process for cooperation with other image processing software. Another limitation is the noise, which is noticeable as roughness in the three-axis DKI-H. This might be due to the miscalculation of MK values at each pixel, because the artifact for the signal value at each pixel of the acquired DW image becomes stronger in the three-axis average than in the 30-axis average. The effectiveness of noise reduction by a pre- or post-processing filter [31-35] should be examined against the increase in noise due to the decreased

amount of information as a result of this short-time imaging. Although filter processing is necessary to overcome the noise from insufficient signals of DW images captured with three *b*-values, it could change some MK values in the DK images. A clinical trial (approval no. RIN2011-041) has been initiated to test the effect of several types of filter processing on the diagnostic ability of our new software for some diseases, and the software including filter processing will be released after the completion of this trial.

In conclusion, the DK images that were created by the new software and short-time imaging sequences were similar to the original DK images created by long-time imaging sequences. The use of this software might allow any medical facility to easily conduct clinical research and use daily clinical applications of DK imaging.

Acknowledgments. We thank the staff of the Department of Radiology and the Central Division of Radiology at Okayama University Hospital for their support of this study. The study was supported by Grants-in-Aid for Scientific Research (nos. C22591335, 15K09924 and 19K0809801) from the Ministry of Health, Labour and Welfare of Japan.

References

1. Lutsep HL, Albers GW, DeCrespigny A, Kamat GN, Marks MP and Moseley ME: Clinical utility of diffusion-weighted magnetic resonance imaging in the assessment of ischemic stroke. Ann Neurol (1997) 41: 574–580.
2. van Everdingen KJ, van der Grond J, Kappelle LJ, Ramos LMP and Mali WPTM: Diffusion-weighted magnetic resonance imaging in acute stroke. Stroke (1998) 29: 1783–1790.
3. Guo Y, Cai YQ, Cai ZL, Gao YG, An NY, Ma L, Mahankali S and Gao JH: Differentiation of clinically benign and malignant breast lesions using diffusion-weighted imaging. J Magn Reson Imaging (2002) 16: 172–178.
4. Tamada T, Sone T, Jo Y, Toshimitsu S, Yamashita T, Yamamoto A, Tanimoto D and Ito K: Apparent diffusion coefficient values in peripheral and transition zones of the prostate: comparison between normal and malignant prostatic tissues and correlation with histologic grade. J Magn Reson Imaging (2008) 28: 720–726.
5. Hui ES, Fieremans E, Jensen JH, Tabesh A, Feng W, Bonilha L, Spampinato MV, Adams R and Helpern JA: Stroke assessment with diffusional kurtosis imaging. Stroke (2012) 43: 2968–2973.
6. Wang JJ, Lin WY, Lu CS, Weng YH, Ng SH, Wang CH, Liu HL, Hsieh RH, Wan YL and Wai YY: Parkinson disease: diagnostic utility of diffusion kurtosis imaging. Radiology (2011) 261: 210–217.
7. Arab A, Wojna-Pelczar A, Khairnar A, Szabó N and Ruda-Kucerova J: Principles of diffusion kurtosis imaging and its role in early diagnosis of neurodegenerative disorders. Brain Res Bull (2018) 139: 91–98.
8. Tamura C, Shinmoto H, Soga S, Okamura T, Sato H, Okuaki T, Pang Y, Kosuda S and Kaji T: Diffusion kurtosis imaging study of prostate cancer: preliminary findings. J Magn Reson Imaging (2014) 40: 723–729.
9. Liu C, Xing Y, Wei D, Jiao Q, Yang Q, Lei D, Tao X and Yao W: Diffusion kurtosis imaging as a prognostic marker in osteosarcoma patients with preoperative chemotherapy. Biomed Res Int (2020) 2020: 3268138.
10. Hempel JM, Schittenhelm J, Bisdas S, Brendle C, Bender B, Bier G, Skardelly M, Tabatabai G, Vega SC, Ernemann U and Klose U: In vivo assessment of tumor heterogeneity in WHO 2016 glioma grades using diffusion kurtosis imaging: diagnostic performance and improvement of feasibility in routine clinical practice. J Neuroradiol (2018) 45: 32–40.
11. Wang J, Dou W, Shi H, He X, Wang H, Ge Y and Cheng H: Diffusion kurtosis imaging in liver: a preliminary reproducibility study in healthy volunteers. Magn Reson Mat Phys Biol Med (2020) 33: 877–883.
12. Jensen JH and Helpern JA: MRI quantification of non-Gaussian water diffusion by kurtosis analysis. NMR Biomed (2010) 23: 698–710.
13. Matsumoto Y, Kuroda M, Matsuya R, Kato H, Shibuya K, Oita M, Kawabe A, Matsuzaki H, Asaumi J, Murakami J, Katashima K, Ashida M, Sasaki T, Sei T, Kanazawa S, Mimura S, Oono S, Kitayama T, Tahara S and Inamura K: In vitro experimental study of the relationship between the apparent diffusion coefficient and changes in cellularity and cell morphology. Oncol Rep (2009) 22: 641–648.
14. Katashima K, Kuroda M, Ashida M, Sasaki T, Taguchi T, Matsuzaki H, Murakami J, Yanagi Y, Hisatomi M, Hara M, Kato H, Ohmura Y, Kobayashi T, Kanazawa S, Harada S, Takemoto M, Ohno S, Mimura S and Asaumi J: In vitro assessment of factors affecting the apparent diffusion coefficient of Jurkat cells using bio-phantoms. Acta Med Okayama (2013) 67: 359–367.
15. Khasawneh A, Kuroda M, Yoshimura Y, Sugianto I, Bamgbose BO, Hamada K, Barham M, Tekiki N, Konishi K, Sugimoto K, Ishizaka H, Kurozumi A, Matsushita, T, Ohno S, Kanazawa S and Asaumi J: Development of a novel phantom using polyethylene glycol for the visualization of restricted diffusion in diffusion kurtosis imaging and apparent diffusion coefficient subtraction method. Biomed Rep (2020) 13: 52.
16. Yoshimura Y, Kuroda M, Sugianto I, Bamgbose BO, Miyahara K, Ohmura Y, Kurozumi A, Matsushita T, Ohno S, Kanazawa S and Asaumi J: The usefulness of readout-segmented echo-planar imaging (RESOLVE) for bio-phantom imaging using 3-tesla clinical MRI. Acta Med Okayama (2018) 72: 53–59.
17. Yoshimura Y, Kuroda M, Sugianto I, Khasawneh A, Bamgbose BO, Hamada K, Barham M, Tekiki N, Kurozumi A, Matsushita T, Ohno S, Kanazawa S and Asaumi J: Development of a novel method for visualizing restricted diffusion using subtraction of apparent diffusion coefficient values. Mol Med Rep (2019) 20: 2963–2969.
18. Chu JP, Song YK, Tian YS, Qiu HS, Huang XH, Wang YL, Huang YQ and Zhao J: Diffusion kurtosis imaging in evaluating gliomas: different region of interest selection methods on time efficiency, measurement repeatability, and diagnostic ability. Eur Radiol (2021) 31: 729–739.
19. Sun Q, Fan W, Liu Y, Zou Y, Wiseman N, Kou Z and Han P: Characterization of brain microstructural abnormalities in cirrhotic patients without overt hepatic encephalopathy using diffusion kurtosis imaging. Brain Imaging Behav (2020) 14: 627–638.
20. Chenevert TL, Stegman LD, Taylor JMG, Robertson PL, Greenberg HS, Rehemtulla A and Ross BD: Diffusion magnetic

resonance imaging: an early surrogate marker of therapeutic efficacy in brain tumors. J Natl Cancer Inst (2000) 92: 2029–2036.
21. Guan J, Ma X, Geng Y, Qi D, Shen Y, Shen Z, Chen Y, Wu E and Wu R: Diffusion kurtosis imaging for detection of early brain changes in Parkinson's disease. Front Neurol (2019) 10: 1285.
22. Pasicz K, Podgórska J, Jasieniak J, Fabiszewska E, Skrzyński W, Anysz-Grodzicka A, Cieszanowski A, Kukołowicz P and Grabska I: Optimal b-values for diffusion kurtosis imaging of the liver and pancreas in MR examinations. Phys Medica (2019) 66: 119–123.
23. Rosenkrantz A, Padhani A, Chenevert T, Koh D, Keyzer F, Taouli B and Bihan D: Body diffusion kurtosis imaging: Basic principles, applications, and considerations for clinical practice. J Magn Reson Imaging (2015) 42: 1190–1202.
24. Quentin M, Pentang G, Schimmöller L, Kott O, Müller-Lutz A, Blondin D, Arsov C, Hiester A, Rabenalt R and Wittsack H: Feasibility of diffusional kurtosis tensor imaging in prostate MRI for the assessment of prostate cancer: Preliminary results. Magn Reson Imaging (2014) 32: 880–885.
25. Vargas H, Lawrence E, Mazaheri Y and Sala E: Updates in advanced diffusion-weighted magnetic resonance imaging techniques in the evaluation of prostate cancer. World J Radiol (2015) 7: 184–188.
26. Fu J, Ye J, Zhu W, Wu J, Chen W and Zhu Q: Magnetic resonance diffusion kurtosis imaging in differential diagnosis of benign and malignant renal tumors. Cancer Imaging (2021) 21: 6.
27. Zhu Q, Xu Q, Dou W, Zhu W, Wu J, Chen W and Ye J: Diffusion kurtosis imaging features of renal cell carcinoma: A preliminary study. Br J Radiol (2021) 94: 20201374. DOI 10.1259/bjr.20201374.
28. Zhu J, Luo X, Gao J, Li S, Li C and Chen M: Application of diffusion kurtosis tensor MR imaging in characterization of renal cell carcinomas with different pathological types and grades. Cancer Imaging (2021) 21: 30.
29. Wu C, Zhang Y, Bao M, Li H, Wang X, Liu X and Shi H: Diffusion kurtosis imaging helps to predict upgrading in biopsy-proven prostate cancer with a Gleason score of 6. AJR Am J Roentgenol (2017) 209: 1081–1087.
30. Zhang Y, Wu C, Bao M, Li H, Yan X, Liu X and Shi H: New RESOLVE-based diffusional kurtosis imaging in MRI-visible prostate cancer: Effect of reduced b value on image quality and diagnostic effectiveness. AJR Am J Roentgenol (2016) 207: 330–338.
31. Zhou MX, Yan X, Xie HB, Zheng H, Xu D and Yang G: Evaluation of non-local means based denoising filters for diffusion kurtosis imaging using a new phantom. PLOS ONE (2015) 10: 2.
32. Madhyastha T, Mérillat S, Hirsiger S, Bezzola L, Liem F, Grabowski T and Jäncke L: Longitudinal reliability of tract-based spatial statistics in diffusion tensor imaging. Hum Brain Mapp (2014) 35: 4544–4555.
33. Yang J, Fan J, Ai D, Zhou S, Tang S and Wang Y: Brain MR image denoising for Rician noise using pre-smooth non-local means filter. Biomed Eng Online (2015) 14: 2.
34. Masutani Y and Aoki S: Fast and robust estimation of diffusional kurtosis imaging (DKI) parameters by general closed-form expressions and their extensions. Magn Reson Med Sci (2014) 13: 97–115.
35. Gonzalez RC and Woods RE: Image enhancement in the spatial domain; in Digital Image Processing, 2nd Ed, Prentice Hall, New Jersey (2002) pp 123–124.

Evaluation of Fast Diffusion Kurtosis Imaging Using New Software Designed for Widespread Clinical Use

ORIGINALITY REPORT

13%	11%	9%	2%
SIMILARITY INDEX	INTERNET SOURCES	PUBLICATIONS	STUDENT PAPERS

PRIMARY SOURCES

1	tessera.spandidos-publications.com Internet Source	3%
2	spandidos-publications.com Internet Source	1%
3	eprints.lib.okayama-u.ac.jp Internet Source	1%
4	IFMBE Proceedings, 2013. Publication	1%
5	www.spandidos-publications.com Internet Source	1%
6	wjso.biomedcentral.com Internet Source	<1%
7	iovs.arvojournals.org Internet Source	<1%
8	Submitted to iGroup Student Paper	<1%
9	www.mhlw.go.jp Internet Source	<1%

10	Takashi Koyama. "Functional MR imaging of the female pelvis", Journal of Magnetic Resonance Imaging, 06/2007 Publication	<1 %
11	Submitted to China Medical University, Taiwan Student Paper	<1 %
12	Lukas Kaufmann, Claudia Marcolli, Beiping Luo, Thomas Peter. "Refreeze experiments of water droplets containing different types of ice nuclei interpreted by classical nucleation theory", Copernicus GmbH, 2016 Publication	<1 %
13	bmcoralhealth.biomedcentral.com Internet Source	<1 %
14	www.nature.com Internet Source	<1 %
15	bio-protocol.org Internet Source	<1 %
16	doaj.org Internet Source	<1 %
17	Babatunde O. Bamgbose, Shunsuke Okada, Miki Hisatomi, Yoshinobu Yanagi et al. "Fourth molar: A retrospective study and literature review of a rare clinical entity", Imaging Science in Dentistry, 2019 Publication	<1 %

18	www.freepatentsonline.com Internet Source	<1 %
19	Winnie Wan Yee Tso, Edward Sai Kam Hui, Tatia Mei Chun Lee, Anthony Pak Yin Liu et al. "Brain Microstructural Changes Associated With Neurocognitive Outcome in Intracranial Germ Cell Tumor Survivors", Frontiers in Oncology, 2021 Publication	<1 %
20	pubs.rsna.org Internet Source	<1 %
21	"ECR 2018 - BOOK OF ABSTRACTS", Insights into Imaging, 2018 Publication	<1 %
22	Junichiro Sakamoto, Ami Kuribayashi, Shinya Kotaki, Mamiko Fujikura, Shin Nakamura, Tohru Kurabayashi. "Application of diffusion kurtosis imaging to odontogenic lesions: Analysis of the cystic component", Journal of Magnetic Resonance Imaging, 2016 Publication	<1 %
23	Kuroda, . "A new phantom using polyethylene glycol as an apparent diffusion coefficient standard for MR imaging", International Journal of Oncology, 2009. Publication	<1 %
	jcancer.org	

24	Internet Source	<1%
25	researchmap.jp Internet Source	<1%
26	tel.archives-ouvertes.fr Internet Source	<1%
27	www.ajronline.org Internet Source	<1%
28	Baikeev, Rustem F, Roman A Gubanov, Kamil K Sadikov, Sufiya Z Safina, Farhat F Muhamadiev, and Timur A Sibgatullin. "Dynamic properties of water in breast pathology depend on the histological compounds: distinguishing tissue malignancy by water diffusion coefficients", BMC Research Notes, 2014. Publication	<1%
29	Jiangyang Zhang, Peter C.M. van Zijl, Susumu Mori. "Image contrast using the secondary and tertiary eigenvectors in diffusion tensor imaging", Magnetic Resonance in Medicine, 2006 Publication	<1%
30	Jing Wang, Chen-Jiang Wu, Mei-Ling Bao, Jing Zhang, Xiao-Ning Wang, Yu-Dong Zhang. "Machine learning-based analysis of MR radiomics can help to improve the diagnostic	<1%

performance of PI-RADS v2 in clinically relevant prostate cancer", European Radiology, 2017
Publication

31	cancerimagingjournal.biomedcentral.com Internet Source	<1 %
32	oem.bmj.com Internet Source	<1 %
33	qims.amegroups.com Internet Source	<1 %
34	vuir.vu.edu.au Internet Source	<1 %
35	www.dovepress.com Internet Source	<1 %
36	www.wjgnet.com Internet Source	<1 %
37	Ke Yang, Xiao-Ming Zhang, Lin Yang, Hao Xu, Juan Peng. "Advanced imaging techniques in the therapeutic response of transarterial chemoembolization for hepatocellular carcinoma", World Journal of Gastroenterology, 2016 Publication	<1 %
38	blog.response.restoration.noaa.gov Internet Source	<1 %

Exclude quotes	On	Exclude matches	< 5 words
Exclude bibliography	On		